NIST Advanced Manufacturing Series 100-16

Literature Review of Metal Additive Manufacturing Defects

Felix H. Kim
Shawn P. Moylan

This publication is available free of charge from:
https://doi.org/10.6028/NIST.AMS.100-16

National Institute of Standards and Technology
U.S. Department of Commerce

NIST Advanced Manufacturing Series 100-16

Literature Review of Metal Additive Manufacturing Defects

Felix H. Kim
Shawn P. Moylan
Engineering Laboratory

This publication is available free of charge from:
https://doi.org/10.6028/NIST.AMS.100-16

May 2018

U.S. Department of Commerce
Wilbur L. Ross, Jr., Secretary

National Institute of Standards and Technology
Walter Copan, NIST Director and Undersecretary of Commerce for Standards and Technology

Abstract

Additive manufacturing (AM) is a revolutionary manufacturing technique, which is expected to reshape the future of manufacturing industries. While various materials are used in AM, metal AM is expected to provide a high impact to the industry by producing high-strength structural components. Defects occurring in metal AM, however, prevent the technique from a wide spread adoption by the mainstream industry. This paper provides a review of commonly-occurring defects in metal AM-produced components. It describes various types and causes of defects, and provides implications on the needs of non-destructive evaluation (NDE) techniques to inspect such defects.

Key words

Additive Manufacturing; Cracks; Defect; Metal; Porosity; Residual Stress.

Disclaimer

Commercial equipment and materials are identified in order to adequately specify certain procedures. In no case does such identification imply recommendation or endorsement by the National Institute of Standards and Technology, nor does it imply that the materials or equipment identified are necessarily the best available for the purpose.

Table of Contents

List of Figures

1. Introduction

Additive Manufacturing (AM) is a revolutionary manufacturing process producing near-net shape of various materials (polymers, ceramics, and metals). ASTM International has defined additive manufacturing as “a process of joining materials to make objects from 3D model data, usually layer upon layer, as opposed to subtractive manufacturing methodologies Synonyms: additive fabrication, additive processes, additive techniques, additive layer manufacturing, layer manufacturing, and freeform fabrication” [1, 2]. Metal AM generally builds a part using a layer-wise process with feedstock materials in the form of powder, wire, or sheet. Energy sources such as laser beam, electron beam, arc, or ultrasound are currently utilized in metal AM. In this paper, laser-based and electron beam melting (EBM)-based metal AM methods will be focused. Two types of techniques are available for laser-based metal AM: powder-bed fusion (PBF) and directed energy deposition (DED). EBM-based technique involves PBF or wire feed type of processes. Both PBF and DED-based techniques mainly use metal powders as the feed stock material. The DED technique can also use metal wire as a feed stock material. Details on the metal AM methods and associated techniques can be obtained from recent reviews [1, 3-5].

As the AM methods are relatively new with various emerging techniques and materials involved, research activities have been scattered without comprehensive and standardized tests. At the same time, AM methods and associated techniques have made significant progress during the last decade. The National Research Council (NRC) has identified significant needs for researching, identifying, developing, and gaining consensus on standard qualification and certification methodologies for different applications in AM [6]. Recently, The National Institute of Standards and Technology (NIST) has brought together research communities and industries to create a measurement science roadmap for metal-based additive manufacturing [7]. NIST specifically identified some of the challenges of AM including characterization of the raw materials, process monitoring, and finished part inspection.

Metal AM is still at its early stage of development, and the fundamental processing-microstructure-property relationships are not fully understood. Without optimized processing parameters, defects can often occur in parts produced with AM. These defects can potentially lead to failures of AM parts. The microstructure has a direct effect on a material’s physical and mechanical properties, and several researchers investigated the microstructure of AM parts and the effects of manufacturing parameters, some of which will be reviewed in this paper. Proper measurements of mechanical properties are also crucial, and anisotropy associated with manufacturing direction has been investigated recently.

While there are various materials being explored for metal AM, NIST has focused on Stainless Steel, Nickel alloy (IN 625), Cobalt Chromium alloy (CoCr), Titanium alloy (Ti6-Al4-V), and Aluminum (Al). More research has been performed around Titanium-based AM parts than other materials due to applications in medical and aerospace fields. Recently, increasing research on Stainless Steel was observed during the literature review process. For some materials (IN 625, CoCr, and Al), limited literature was available at

the time of this review. This fact indicates opportunities and needs for NIST and others to perform more research for these important materials.

The reviewed literature presented various types of defects occurring for different materials and manufacturing methods/techniques. The manufacturing parameters affecting the microstructural defects were also identified. Several different AM techniques were used, which included laser and electron beam-based DED and PBF. The AM research involves and requires understanding from various disciplines: material science, material characterization, process engineering, and manufacturing, to name a few. The problems identified by researchers included microscopic and mesoscale defects (porosity) as well as limitations in mechanical properties (reduced elongation and residual stress). Some of these defects will be further investigated with X-ray Computed Tomography (XCT) or other relevant measurement techniques.

2. Porosity

Pores in an AM part can be either undesirable defects in the solid phase contributing to the failure of the system or intentionally designed pore structures for special applications. Characterizations of both types of porosity are important to predict mechanical properties of the structure. In this paper, we are focusing on the pores as defects.

The overall porosity of the solid phase is now at a level of about 1 % to 5 % for some materials due to improvements in process optimization [e.g., 8]. While the bulk porosity value may be low, the individual pore size and shape can be a trigger for a catastrophic failure. Optimization of processing parameters to reduce porosity can also be a lengthy process for new AM processes and materials. This type of porosity can be classified as two types in AM-produced parts: lack-of-fusion (LOF) porosity and gas porosity.

The LOF porosity occurs due to a poor choice of processing parameters. Vandenbroucke and Kruth showed optical micrographs of a parametric study for Ti-6Al-4V [9]. The author did not describe the orientation of the microscopic images acquired, but it is assumed to be orthogonal to the build direction based on the alignment of pores. The hatch spacing and scan speed were varied to understand the effect on microstructure. They demonstrated that the density of Ti-6Al-4V is highly repeatable and controllable through the processing parameters, up to a density of 99.98 % using a higher energy density input. The figure shows how a poor choice of processing parameters can produce pores with irregular shapes along the hatch track or between layers. Yadroitsev et al. also studied the effect of hatch distance on porosity, as shown in Fig. 1 [10]. They found an optimum value of hatch spacing to minimize porosity, which was approximately equal to the actual width of the hatch track. While the laser spot size was 70 µm, the actual width of an individual hatch was found to be 120 µm, which was also found to be the optimum hatch spacing distance to minimize porosity. Mireles et al. designed artificial defects in a part, and monitored the build with in-situ thermography [11]. The part was later compared to XCT measurements. They applied a re-scanning strategy in the region with the defect, which successfully eliminated pores.

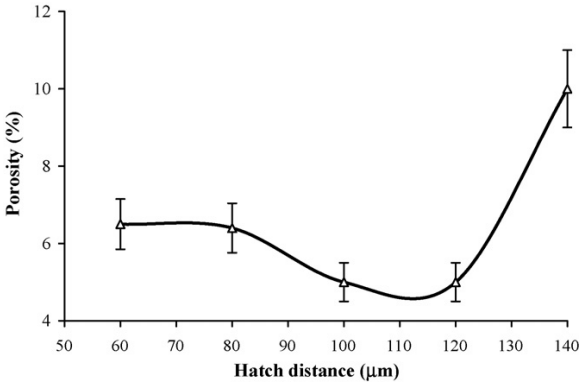

Fig. 1. Samples porosity vs. hatch distance. Inconel 625 powder, powder layer thickness 50 μm, laser power 50 W, laser spot size d ≈ 70 μm, V = 0.13 m/s (Reproduced from [10], with permission from Elsevier).

Gas pores, on the other hand, are spherical pores occurring due to gas trapped in the raw metal powder particles or trapped environmental inert gas during the melting process. The causes of gas pores are still in discussion. Ng et al. demonstrated the presence of pores within gas-atomized metal powder particles as the cause of gas pores in a produced part after solidification [12]. Unlike LOF porosity, gas porosity is more difficult to eliminate, which can be as high as 0.7 % according to Ng. et al. Pores in gas atomized powders are shown in a cross-sectional optical image of powder particles, and the resulting pores in a laser deposit are shown in Fig. 2. In addition, the effects of buoyancy-driven flow and Marangoni-driven flow for a gas bubble was theoretically compared, which showed that the gas bubble is likely to be retained in the melt pool due to stronger effect of the Marangoni-driven flow. Gas bubbles tend to coalesce to form a larger pore than an individual gas bubble would create. Kobryn et al. found that both LOF and gas porosity decreased with increasing scan speed and power level [13]. Murr et al. showed that the two types of pores can coexist in a single part with scanning electron microscopy (SEM) images, as shown in Fig. 3 [14]. Li found a gas pore with a diameter of approximately 80 μm, and a LOF pore with irregular shape about 400 μm in size [15]. He found that baking the feedstock powder immediately before deposition tends to significantly reduce the formation of spherical pores. Increasing the laser heat input also reduced the formation of gas pores by decreasing the solidification rate, which increased the chance of gaseous phase to escape to the atmosphere before a melt pool solidifies. Ahsan et al. demonstrated that the gas atomization process tends to produce more internal porosity in the powders compared to the powders produced with a plasma rotating electrode process (PREP), as shown in Fig. 4 from XCT images, which results in higher amounts of gas porosity in the finished part [16].

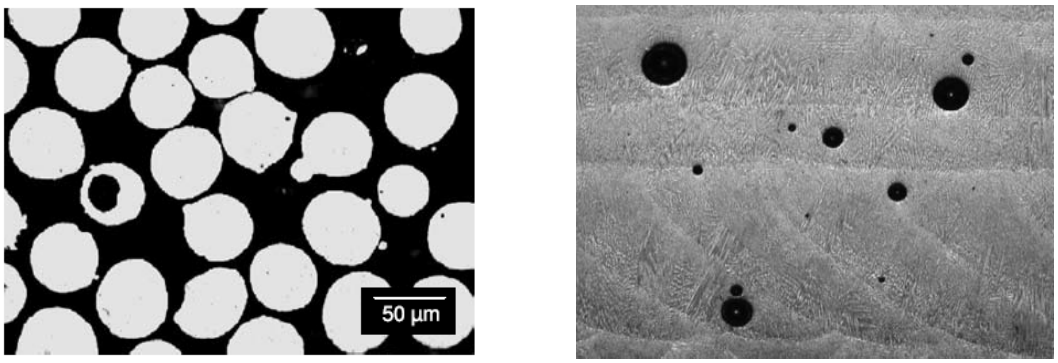

(a) (b)

Fig. 2. Optical micrographs of (a) gas atomized powders showing pores within the powders and (b) cross-section of a laser deposit showing high level of gas porosity (Reproduced from [12] with permission of Springer).

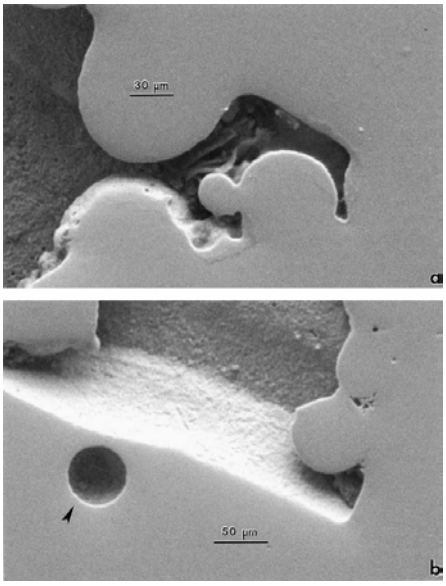

Fig. 3. SEM views of a polished and unetched horizontal section from a test block, showing unconsolidated and unmelted regions creating porosity in (a) and (b) and a remnant Ar bubble section at arrow in (b) (Reproduced from [14], with permission of Elsevier).

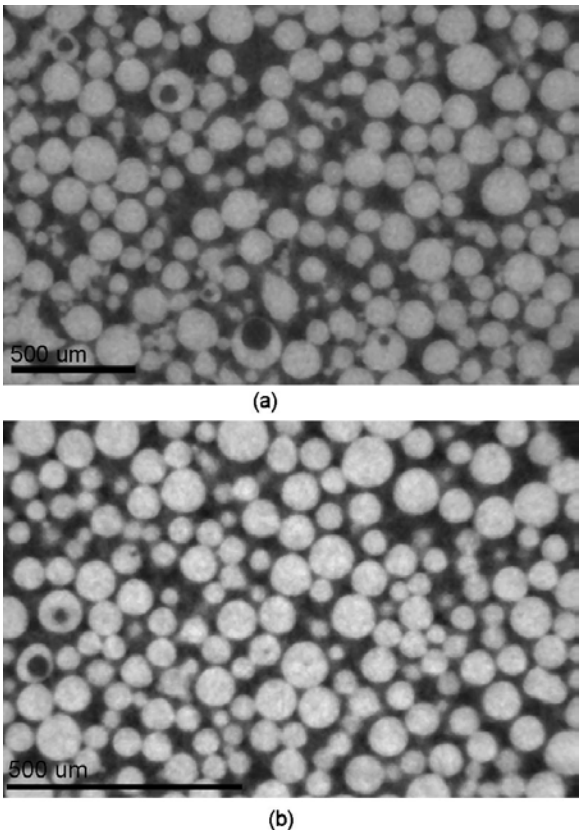

Fig. 4. MicroCT images at a particular slice of (a) gas-atomized powder and (b) PREP powder (Reproduced from [16], with the permission of the Laser Institute of America).

Similar to the work of Yadroitsev et al. [10], Thijis et al. not only found that the angle of epitaxial grain growth depends on the hatch spacing, but also showed that LOF pores were aligned at this angle, as shown in Fig. 5c and g [17]. One of the experiments incorporated a strategy of scanning laser from right to left, and the experiment confirmed that the grain growth direction was toward the meltpool (at an angle toward left when viewed from the side). Pores are also visible along the hatches, as shown in Fig. 5a and e.

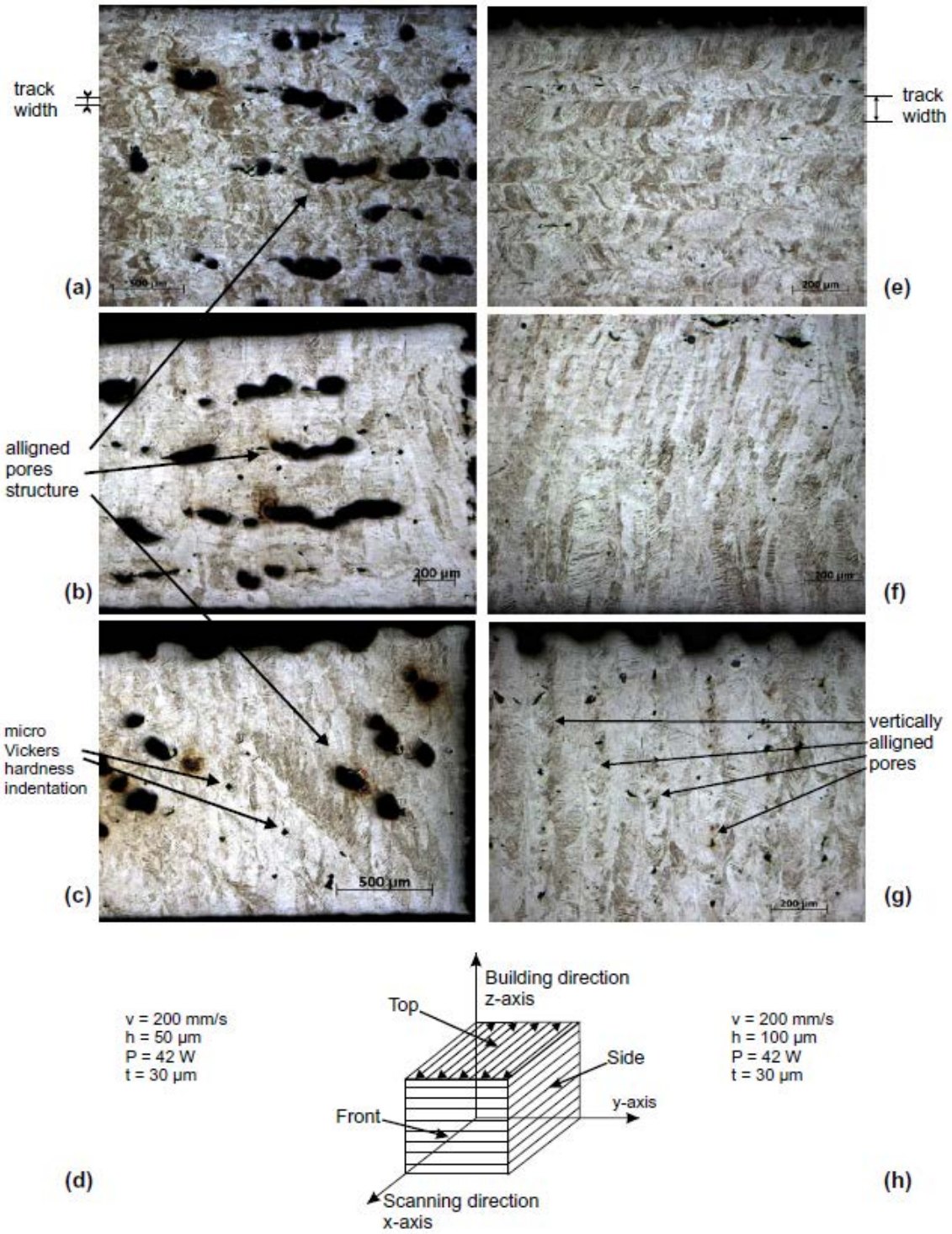

Fig. 5. Influence of hatch spacing. Micrographs of a sample scanned with a hatch spacing of 50 µm: (a) top view; (b) side view; (c) front view; and (d) the scanning strategy and parameters applied. Micrographs of a sample scanned with a hatch spacing of 100 µm: (e) top view; (f) side view; (g) front view; and (h) the scanning strategy and parameters applied (Reproduced from [17], with permissions from Elsevier).

In summary, the formation of gas pores is related to feedstock material quality and gas-assisted powder delivery process (e.g., as in DED). The gas pores are spherical in shape, and the sizes vary from a few micrometers to 100 μm. On the other hand, LOF pores are formed due to poor choice of processing parameters. The LOF pores are generally non-spherical in shape, and the size depends on the set of processing parameters chosen. The gas pores are inherently formed in a single melt pool, and it is generally difficult to detect with an in-situ monitoring system. The LOF pores can show an early sign of formation at a given layer, and therefore there is a potential for early detection with in-situ monitoring of each layer.

3. Porosity and Mechanical Properties

A pore in a part can be a failure initiation point, and it is desirable to reduce porosity in a manufactured component. Sercombe et al. revealed pores up to ≈ 500 μm in Ti-6Al-7Nb parts, which were concluded as possible sources of preferential crack nucleation and propagation [18]. The x-y plane is defined parallel to the surface of the manufacturing stage. The stage motion occurs in the (negative) z-direction in 50 μm increments, with the most recently produced layer being at the top. They have also compared microstructures obtained from different heat treatment processes. This type of pore is expected to reduce the fatigue life span, and they concluded that developing a microstructure resistant to crack propagation would be beneficial.

The detrimental effect of non-spherical morphology of LOF defects to fatigue life was demonstrated by Liu et al. [19]. LOF defects were revealed from fractography, and these were found to be responsible for fatigue crack initiation. The reduction of fatigue life was affected by the location, size, and shape of the LOF defect.

Gong et al. tried to characterize LOF defect morphologies using micrograph images with image processing techniques [20]. Then, in another paper, Gong et al. demonstrated that gravimetric density measurement alone does not necessarily describe the mechanical performance, as shown in Fig. 6 and Fig. 7 [21]. Parts produced with energy densities lower and higher than the optimum value could result in the same density, but the actual mechanical performances would be different as the former may have trapped unmelted powders that contributed to the density measurement. The samples were produced with a laser-based PBF (L-PBF) process. The sample produced with optimum processing parameters, L-PBF-OP1, received an energy density of 42 J/mm^3, and the samples produced with modified parameters, L-PBF-MP2 through 5, had energy densities of 74, 100, 32, and 27 J/mm^3, respectively. The L-PBF-OP1 sample resulted in 0 % porosity, and L-PBF-MP2 – 6 had porosities of 1 %, 5 %, 1 %, and 5 %, respectively.

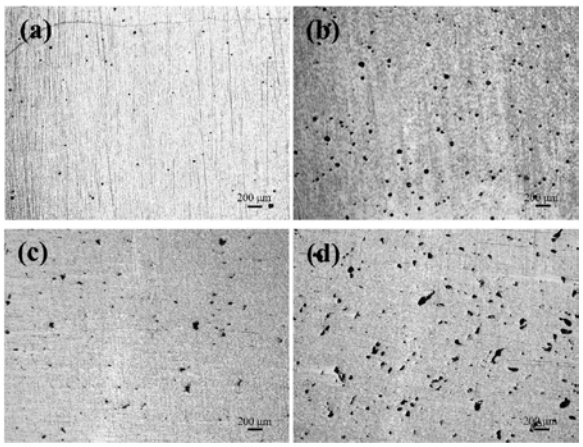

Fig. 6. Optical micrographs of L-PBF samples in as-polished condition: (a) L-PBF-MP2, (b) L-PBF-MP3, (c) L-PBF-MP4, (d) L-PBF-MP5 (Reproduced from [21], with permission of Elsevier).

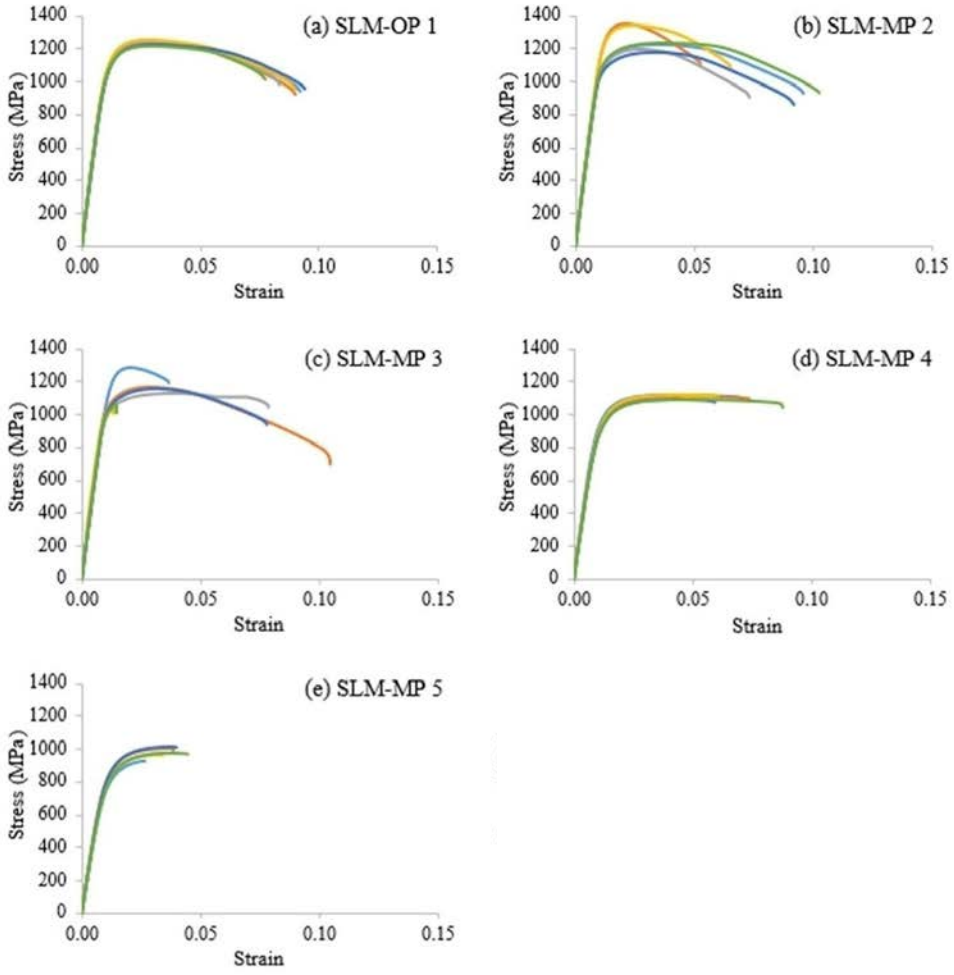

Fig. 7. Stress–strain plots of L-PBF-produced Ti–6Al–4 V specimens (Reproduced from [21] with permission of Elsevier).

Wycisk et al. performed high cyclic fatigue (HCF) tests up to 10^9 cycles [22]. As predicted by Murakami criteria for surface interaction [23], cracks initiated from the surface in the low cycled tests while cracks initiated from the internal defect in the high cycled test, as shown in Fig. 8. Internal defects with 500 µm or larger significantly reduced the number of cycles to failure (N_f) and led to an early failure. Hot-isostatic-pressing was applied and found to improve fatigue strength. Leuders et al. also found that internal pores have a drastic effect on the fatigue behavior in the HCF regime [24].

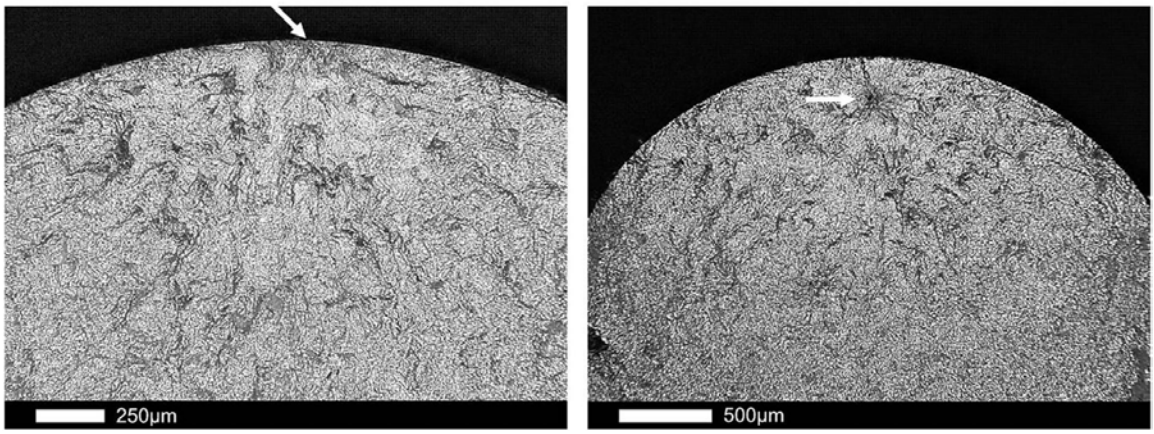

Fig. 8. Crack initiation site for hot-isostatic-pressed specimen under tension–tension loading; surface crack initiation at $N_f = 2.9 \times 10^5$ (left) and internal crack initiation at $N_f = 2.4 \times 10^6$ (right). N_f refers to the cycle at failure. (Reproduced from [22], with permission of the original authors)

Zhang et al. investigated an AM part (Ti-24Nb-4Zr-8Sn) produced by L-PBF [25]. The material had lower modulus which was more compatible with that of a human bone than that of more popular Ti-6Al-4V. As the laser scan speed decreases (down to ≈ 600 mm/s), the relative density and Vickers hardness test values increase. The relative densities and Vickers hardness values again decrease at much lower speeds (300 mm/s). The strength and modulus were independent of the scan speeds. The ductility was greatly affected by the scan speeds. Cracks were initiated at defects (e.g., around the poorly-bonded grains). More defects and powders not fully melted were visible, and the fracture surface showed a mixture of smooth zones and elongated dimple fractures.

4. Residual Stress

Residual stress is present in many manufactured parts, and has been a critical problem in the industry. Shiomi et al. measured residual stress of AM layers made from chrome molybdenum steel powder mixed with copper phosphate and nickel powders using the L-PBF process [26]. The L-PBF system used a pulsed Nd-YAG laser with a maximum average power of 50 kW and peak power of 3 kW. The model is built on a base plate in the chamber filled with nitrogen gas. A strain gauge is attached at the center of the bottom surface of the base plate. Each layer of the model is removed, and the strain is measured to estimate residual stress. Young's modulus of 50 GPa determined from a tension test for the model and 200 GPa for the stainless base plate was used for estimation. Residual stress up to 500 MPa was observed at the top layer of the model.

The scan speed did not affect the residual stress significantly. It was discovered that the residual stress can be relieved by heating the part higher than 600 ^{o}C after placing a part in the furnace for an hour. Based on the discovery, the top surface was re-scanned, and the residual stress in the top layer decreases as the energy input in re-scanning increases. It was also considered that a higher cooling speed may have caused a larger residual stress. The powder bed temperature was raised by heating the base plate. The residual stress in the top layer decreased as the temperature of the base plate was raised.

Wu et al. measured residual stress of an AM part (316L Stainless Steel) using both digital image correlation (DIC) and neutron diffraction techniques [27]. They studied the effects of laser scanning pattern, power, speed, and build direction in L-PBF AM on residual stress. 316L stainless steel powder with a 30 µm powder layer was used to produce L-shaped rectangular and quadrilateral prism specimens. The 5 mm × 5 mm island scanning strategy was adopted for preparation of the L-shaped specimens. Neutron diffraction measurements were performed on the Spectrometer for Materials Research at Temperature and Stress (SMARTS) diffractometer at the Lujan Center at Los Alamos Neutron Science Center (LANSCE), Los Alamos National Laboratory. DIC measurements were performed using a noncontact optical measurement system to evaluate the strain resulting from sectioning and build plate removal. Specked patterns on the images before and after were compared digitally to evaluate strain on a facet size of 100 pixels. The DIC results provide surface level residual stress relief, and the Neutron Diffraction measurements provide interior residual stress level, as shown in Fig. 9. Neutron diffraction measurement revealed significant in-plane residual stresses near the top of the specimen. There was also a significant tensile component on one side of the specimen which could be due to post-process surface polishing on the face or a bending moment within the vertical specimen. Neutron diffraction results on the L-shaped specimen showed the geometry effect on residual stress development. The effect of scan strategies (Island size and Island rotation) and laser power were investigated.

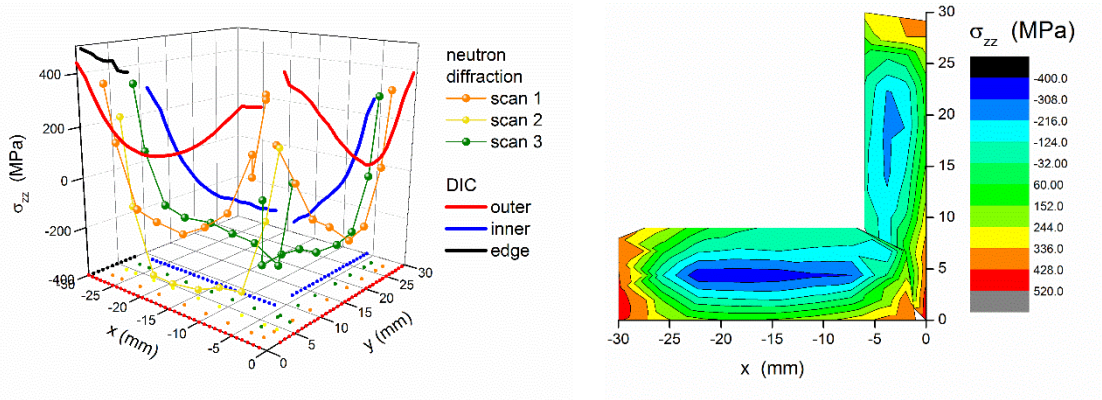

(a) (b)

Fig. 9. Comparison of surface and volumetric axial residual stresses measured via DIC/sectioning and neutron diffraction, respectively, at z = 15 mm in an L-shaped bracket specimen built at 400 W and 1800 mm/s shown as a (a) 3D and (b) contour plot (Reproduced from [27], with permission of Springer).

5. Conclusions and Future Work

As AM becomes a viable alternative manufacturing technique for metal parts, it is important to be able to identify and perform a proper inspection of defects prior to the parts being put into service. The literature review in this paper covered several types of commonly occurring defects. While many mechanical properties (e.g., tensile strength and modulus) of AM-produced components were superior to the parts produced with other techniques, porosity found in the parts was considered to be the main cause of the reduced elongation. The two types of porosity in AM were identified as LOF and gas porosities, and both types of porosities can be formed in a single part. The fatigue strength was also significantly affected by the pores in the part as these pores act as failure initiation points. Therefore, it is important to understand the causes of these pores to reduce the formation of porosity, and be able to post-inspect the AM parts for critical defects. XCT is a promising non-destructive evaluation technique to measure porosity. The critical defect criteria in type, size, orientation, and distribution, however, are yet to be determined. Hence, it is also important to understand the mechanical performance of AM-parts and the associated effect of defects (porosity and cracks) to understand critical defect criteria. Several mechanical tests including fatigue tests have been performed to understand this. In addition, the ongoing effort to study and monitor the effect of porosity on fracture using in-situ XCT scans can provide some insights on this complex problem. In-situ mechanical tests with DIC is also a promising technique to reveal stress distribution at the surface of the test specimens, and the results obtained from the test can be complementary to the data obtained from in-situ or ex-situ XCT measurements. The neutron diffraction technique appears to be a viable non-destructive measurement tool for metal AM-produced components due to the neutron's high penetration capability through metals, despite the limited availability and access to neutron diffraction facilities. Well-designed research projects with selected samples can be performed at a neutron diffraction facility to understand the magnitude and distribution of residual stress for selected critical geometries.

References

[1] Frazier WE (2014) Metal Additive Manufacturing: A Review. *Journal of Materials Engineering and Performance* 23(6):1917-1928. https://doi.org/10.1007/s11665-014-0958-z

[2] ASTM International (2012) StandardTerminology for Additive Manufacturing Technologies. (West Conshohocken, PA).

[3] Murr LE, Gaytan SM, Ramirez DA, Martinez E, Hernandez J, Amato KN, Shindo PW, Medina FR, Wicker RB (2012) Metal Fabrication by Additive Manufacturing Using Laser and Electron Beam Melting Technologies. *Journal of Materials Science & Technology* 28(1):1-14. https://doi.org/http://dx.doi.org/10.1016/S1005-0302(12)60016-4

[4] Kruth JP, Levy G, Klocke F, Childs THC (2007) Consolidation phenomena in laser and powder-bed based layered manufacturing. *CIRP Annals - Manufacturing Technology* 56(2):730-759. https://doi.org/http://dx.doi.org/10.1016/j.cirp.2007.10.004

[5] Kruth JP, Leu MC, Nakagawa T (1998) Progress in Additive Manufacturing and Rapid Prototyping. *CIRP Annals - Manufacturing Technology* 47(2):525-540. https://doi.org/http://dx.doi.org/10.1016/S0007-8506(07)63240-5

[6] National Research Council (2014) 3D Printing in Space. Technical Report

[7] National Institute of Standards and Technology (2013) Measurement Science Roadmap for Metal-Based Additive Manufacturing. Technical Report

[8] Choren JA, Heinrich SM, Silver-Thorn MB (2013) Young's modulus and volume porosity relationships for additive manufacturing applications. *Journal of Materials Science* 48(15):5103-5112. https://doi.org/10.1007/s10853-013-7237-5

[9] Vandenbroucke B , Kruth JP (2007) Selective laser melting of biocompatible metals for rapid manufacturing of medical parts. *Rapid Prototyping Journal* 13(4):196-203. https://doi.org/doi:10.1108/13552540710776142

[10] Yadroitsev I, Thivillon L, Bertrand P, Smurov I (2007) Strategy of manufacturing components with designed internal structure by selective laser melting of metallic powder. *Applied Surface Science* 254(4):980-983. https://doi.org/http://dx.doi.org/10.1016/j.apsusc.2007.08.046

[11] Mireles J, Ridwan S, Morton PA, Hinojos A, Wicker RB (2015) Analysis and correction of defects within parts fabricated using powder bed fusion technology. *Surface Topography: Metrology and Properties* 3(3):034002.

[12] Ng GKL, Jarfors AEW, Bi G, Zheng HY (2009) Porosity formation and gas bubble retention in laser metal deposition. *Applied Physics A* 97(3):641-649. https://doi.org/10.1007/s00339-009-5266-3

[13] Kobryn PA, Moore EH, Semiatin SL (2000) The effect of laser power and traverse speed on microstructure, porosity, and build height in laser-deposited Ti-6Al-4V. *Scripta Materialia* 43(4):299-305. https://doi.org/http://dx.doi.org/10.1016/S1359-6462(00)00408-5

[14] Murr LE, Gaytan SM, Ceylan A, Martinez E, Martinez JL, Hernandez DH, Machado BI, Ramirez DA, Medina F, Collins S, Wicker RB (2010) Characterization of titanium aluminide alloy components fabricated by additive manufacturing using electron beam melting. *Acta Materialia* 58(5):1887-1894. https://doi.org/http://dx.doi.org/10.1016/j.actamat.2009.11.032

[15] Li L (2006) Repair of directionally solidified superalloy GTD-111 by laser-engineered net shaping. *Journal of Materials Science* 41(23):7886-7893. https://doi.org/10.1007/s10853-006-0948-0

[16] Ahsan MN, Bradley R, Pinkerton AJ (2011) Microcomputed tomography analysis of intralayer porosity generation in laser direct metal deposition and its causes. *Journal of Laser Applications* 23(2):022009. https://doi.org/doi:http://dx.doi.org/10.2351/1.3582311

[17] Thijs L, Verhaeghe F, Craeghs T, Humbeeck JV, Kruth J-P (2010) A study of the microstructural evolution during selective laser melting of Ti–6Al–4V. *Acta Materialia* 58(9):3303-3312. https://doi.org/http://dx.doi.org/10.1016/j.actamat.2010.02.004

[18] Sercombe T, Jones N, Day R, Kop A (2008) Heat treatment of Ti-6Al-7Nb components produced by selective laser melting. *Rapid Prototyping Journal* 14(5):300-304. https://doi.org/doi:10.1108/13552540810907974

[19] Liu QC, Elambasseril J, Sun SJ, Leary M, Brandt M, Sharp PK (2014) The Effect of Manufacturing Defects on the Fatigue Behaviour of Ti-6Al-4V Specimens Fabricated Using Selective Laser Melting. *Advanced Materials Research* 891-892:1519-1524. https://doi.org/10.4028/www.scientific.net/AMR.891-892.1519

[20] Gong H, Rafi HK, Karthik NV, Starr TL, Stucker BE (2013) Defect Morphology in Ti-6Al-4V Parts Fabricated by Selective Laser Melting and Electron Beam Melting. in *Solid Freeform Fabrication*

[21] Gong H, Rafi K, Gu H, Janaki Ram GD, Starr T, Stucker B (2015) Influence of defects on mechanical properties of Ti–6Al–4 V components produced by selective laser melting and electron beam melting. *Materials & Design* 86:545-554. https://doi.org/http://dx.doi.org/10.1016/j.matdes.2015.07.147

[22] Wycisk E, Siddique S, Herzog D, Walther F, Emmelmann C (2015) Fatigue Performance of Laser Additive Manufactured Ti–6Al–4V in Very High Cycle Fatigue Regime up to 109 Cycles. *Frontiers in Materials* 2(72). https://doi.org/10.3389/fmats.2015.00072

[23] Murakami Y (2002) *Metal fatigue: effects of small defects and nonmetallic inclusions* (Oxford, Elsevier).

[24] Leuders S, Thöne M, Riemer A, Niendorf T, Tröster T, Richard HA, Maier HJ (2013) On the mechanical behaviour of titanium alloy TiAl6V4 manufactured by selective laser melting: Fatigue resistance and crack growth performance. *International Journal of Fatigue* 48:300-307. https://doi.org/http://dx.doi.org/10.1016/j.ijfatigue.2012.11.011

[25] Zhang LC, Klemm D, Eckert J, Hao YL, Sercombe TB (2011) Manufacture by selective laser melting and mechanical behavior of a biomedical Ti–24Nb–4Zr–8Sn alloy. *Scripta Materialia* 65(1):21-24. https://doi.org/http://dx.doi.org/10.1016/j.scriptamat.2011.03.024

[26] Shiomi M, Osakada K, Nakamura K, Yamashita T, Abe F (2004) Residual Stress within Metallic Model Made by Selective Laser Melting Process. *CIRP Annals - Manufacturing Technology* 53(1):195-198. https://doi.org/http://dx.doi.org/10.1016/S0007-8506(07)60677-5

[27] Wu AS, Brown DW, Kumar M, Gallegos GF, King WE (2014) An Experimental Investigation into Additive Manufacturing-Induced Residual Stresses in 316L Stainless Steel. *Metallurgical and Materials Transactions A* 45(13):6260-6270. https://doi.org/10.1007/s11661-014-2549-x